AIAA JOURNAL
Vol. 38, No. 9, September 2000

Discrete Vortex Simulation on the Acoustic Nonlinearity of an Orifice

Xiaodong Jing* and Xiaofeng Sun†
Beijing University of Aeronautics and Astronautics, 100083 Beijing, People's Republic of China

An axisymmetric potential model to study the nonlinear acoustic properties of an orifice in a plate is presented. The vortex shedding process connected closely with the nonlinear acoustic phenomena is described by a discrete vortex method. Some flow details, such as the rolling up of the shed vortex sheet and the forming of the vena contracta, are simulated. For a sinusoidal pressure variation, both the time history and the spectrum of the average velocity through the orifice are computed, and the nonlinear distortion of the average velocity is analyzed from the computed spectrum. In terms of the fundamental harmonic of the average velocity, the nonlinear acoustic impedance of the orifice is calculated. It is found that the acoustic resistance is in excellent agreement with the previous quasi-steady model and that the acoustic reactance decreases with the increasing sound pressure amplitude as revealed by the previous experiments.

Nomenclature

C_c = vena contracta coefficient
M = maximum number of discrete vortex rings
N = number of discrete vortex rings
P = amplitude of the applied sound pressure
p = applied sound pressure
Q = fluctuating volume flux
R = orifice radius
r = radial coordinate
T = period time, $2\pi/\omega$
t = time
$U(n)$ = amplitude of the nth harmonic of u_{av}
u = local axial velocity
u_{av} = average velocity through orifice
u_I = self-induced velocity of discrete vortex ring
v = local radial velocity
x = axial coordinate
z = specific acoustic impedance normalized by $\rho\omega R$
z_r = specific acoustic resistance normalized by $\rho\omega R$
z_x = specific acoustic reactance normalized by $\rho\omega R$
$\Gamma(t)$ = total circulation at time t
Γ_i = circulation of the ith discrete vortex ring
Δ_i = length of the ith segment of vortex sheet
Δt = time step
ξ_i = axial coordinate of the ith discrete vortex ring
ρ = air density
ρ_i = radial coordinate of the ith discrete vortex ring
σ_i = core radius of the ith discrete vortex ring
ϕ = velocity potential
$\phi(n)$ = phase of the nth harmonic of u_{av}
ω = angular frequency

I. Introduction

HELMHOLTZ resonators are extensively used to suppress noise and flow instabilities at high sound pressure levels. In such conditions, the acoustic properties of the resonators are dominated by nonlinearity. Early works[1–4] showed that the nonlinear acoustic impedance of an orifice in a plate, which is in close connection with the resonators, strongly depends on the amplitude of the applied sound wave. During the past decades, the phenomena related to the acoustic nonlinearity of an orifice have received considerable attention. Salikuddin and Ahuja[5] reported that substantial acoustic loss could occur when a sound wave of low frequency and high amplitude transmitted through the orifices in a plate. Flow separation and the formation of vortex rings were observed in flow visualizations[2,5] when high-amplitude sound wave is incident on an orifice. It has been concluded that the absorption mechanism is the conversion of acoustic energy to vortical energy at a sharp edge.[5] Some investigations[6–8] were carried out of the sound absorption at a sharp edge, and it is shown that the process of sound vortex interaction is linear in the presence of mean flow. When there is no mean flow, the conversion of acoustic energy to vortical energy is in general a nonlinear phenomenon. Some theoretical models were also presented to study this nonlinear process, such as those of Cummings and Eversman,[9] Hersh and Rogers,[10] and Melling.[11] These models mainly concentrate on the nonlinear acoustic resistance or acoustic energy loss, which is successfully predicted by means of the introduction of the vena contracta coefficient, although the underlying physical mechanism for such an empirical coefficient is unclear. However, the vortex shedding produced by a sound wave is not sufficiently considered in the aforementioned quasi-steady models. As a result, flow details, such as the formation of the vortex rings and the distortion of the velocity around the orifice, are not described. In particular, the quasi-steady models have not provided us sufficient knowledge on the nonlinear acoustic reactance that is of great importance in the design of Helmholtz resonators. Therefore we believe that the numerical simulation of the vortex shedding is needed for better understanding the energy conversion mechanism, as well as for obtaining some quantitative results describing the nonlinear acoustic properties of an orifice. For such purposes, in this paper, a discrete vortex model based on axisymmetric potential flow is employed to study the nonlinear process of vortex shedding occurring at an orifice in a plate. The rolling up nature of the shedding vortex sheet is successfully simulated in the near field of the orifice, although the motion of the discrete vortex rings tends to be irregular in the far field. The time history and spectrum of the average velocity through the orifice are computed, from which the distortion of the velocity in the orifice is examined. The nonlinear acoustic resistance and acoustic reactance are calculated in terms of the fundamental harmonic of the average velocity. Note that no empirical parameter like the vena contracta coefficient is introduced because the forming process of the vena contracta is automatically included in the present model. A comparison is made between the present and the theoretical results of the nonlinear acoustic resistance obtained by Cummings and Eversman.[9] The excellent agreement between them validates the present numerical method. The present work differs from the previous investigations in two major respects. First, an effort has been made to study some detailed flow characteristics of the acoustic nonlinearity occurring at an orifice by a theoretical model

Received 20 February 1999; presented as Paper 99-1878 at the AIAA/CEAS 5th Aeroacoustics Conference, Bellevue, WA, 10–12 May 1999; revision received 11 November 1999; accepted for publication 15 February 2000.

*Ph.D. Candidate, Department of Jet Propulsion.
†Professor, Department of Jet Propulsion.

based on potential flow. Second, a numerical approach is employed to calculate the nonlinear acoustic reactance, which has not been solved satisfactorily in the previous quasi-steady models.

Discrete vortex methods have been successfully used by many authors[12,13] to simulate two-dimensional separated flow. Some researchers[14,15] also employ discrete vortex methods to study the acoustically induced vortex shedding in two-dimensional flow. For axisymmetric flow, difficulties arise from applying the Kutta condition at a sharp edge. In the present model, where an orifice is in an infinitely extended plate, an analytical method is developed to apply the Kutta condition at the edge of the orifice. The flowfield is also computed by means of an analytical method.

II. Discrete Vortex Model of the Flowfield

As shown in Fig. 1, an orifice is located in an infinitely thin, rigid plate. The radius of the orifice is R. When a fluctuating pressure difference is applied across the plate, there will be vortex shedding at the sharp edge of the orifice due to the effect of viscosity. The characteristics of the flow around the orifice are strongly dependent on the motion of the shed vortices. Consider that the fluctuating pressure is uniformly distributed in the far field and has a sinusoidal time dependency; that is,

$$p = \begin{cases} P\cos(\omega t) & (x < 0,\ x^2 + r^2 \to \infty) \\ 0 & (x > 0,\ x^2 + r^2 \to \infty) \end{cases} \tag{1}$$

The pressure fluctuation can be produced by a low-frequency incident sound. At low frequency, the sound wavelength greatly exceeds the radius of the orifice, and so the flow is assumed to be incompressible in the vicinity of the orifice. The flow is also assumed to be inviscid, and the viscous effect is only taken into consideration by applying the Kutta condition at the orifice edge. At high Reynolds numbers, the free shear layer is very thin. A discrete vortex model is adopted to describe the flow. The shed vortex sheet is represented by an array of discrete vortex rings $[\xi_i(\Gamma_i, t), \rho_i(\Gamma_i, t)]$. According to the Kelvin theorem, the differential equations that govern the motion of the ith vortex ring with ciculation Γ_i are as follows:

$$\frac{\mathrm{d}\xi_i}{\mathrm{d}t} = u(\xi_i, \rho_i) + u_I(\xi_i, \rho_i), \qquad \frac{\mathrm{d}\rho_i}{\mathrm{d}t} = v(\xi_i, \rho_i) \tag{2}$$

By tracing all of the discrete vortex rings, the evolution of the vortex sheet can be calculated.

A. Velocity of the Flowfield

The variables are normalized as

$$\bar{x} = x/R, \quad \bar{r} = r/R, \quad \bar{\phi} = \phi/\omega R^2, \quad \bar{\Gamma} = \Gamma/\omega R^2$$

$$\bar{t} = \omega t, \quad \bar{u} = u/\omega R, \quad \bar{v} = v/\omega R, \quad \bar{p} = p/\rho\omega^2 R^2$$

In Sec. II, the bars are omitted from the nondimensional variables for simplicity. To obtain the velocity potential ϕ_i, which is induced by the ith discrete vortex ring including the effect of the rigid plate and the orifice, we employ the analytical method in Ref. 16. The main points are 1) an image vortex ring is introduced at $(-\xi_i, \rho_i)$ and 2) the presence of an orifice is represented by a distribution of sources and sinks over the area of the orifice. Then, the expression of the velocity potential ϕ_i is

$$\phi_i(x, r; \xi_i, \rho_i) = H(x\xi_i)E_i(x, r; \xi_i, \rho_i) + H(x\xi_i)\hat{E}_i(x, r; \xi_i, \rho_i) + F_i(x, r; \xi_i, \rho_i) \tag{3}$$

where

$$E_i(x, r; \xi_i, \rho_i) = -\frac{1}{2}\,\mathrm{sgn}(x - \xi_i)\Gamma_i\rho_i \times \int_0^\infty \exp(-k|x - \xi_i|)J_0(kr)J_1(k\rho_i)\,\mathrm{d}k \tag{4}$$

$$\hat{E}_i(x, r; \xi_i, \rho_i) = \frac{1}{2}\,\mathrm{sgn}(x + \xi_i)\Gamma_i\rho_i \times \int_0^\infty \exp(-k|x + \xi_i|)J_0(kr)J_1(k\rho_i)\,\mathrm{d}k \tag{5}$$

$$F_i(x, r; \xi_i, \rho_i) = -\frac{1}{\pi}\,\mathrm{sgn}(x)\Gamma_i\rho_i \int_0^\infty\int_0^\infty\int_0^1 \exp(-k|x| - \lambda|\xi_i|) \times J_0(kr)J_1(\lambda\rho_i)\cos ks\cos\lambda s\,\mathrm{d}s\,\mathrm{d}\lambda\,\mathrm{d}k \tag{6}$$

and $H(y)$ is the Heaviside function. Equation (4) expresses the velocity potential induced by the ith discrete vortex ring in free space, Eq. (5) expresses the velocity potential induced by its image in free space, and Eq. (6) expresses the contribution of the orifice. The vortex sheet is represented by N discrete vortex rings. Thus, the velocity potential of the flowfield is due to the superposition of all of the discrete vortex rings. Note that ϕ_i satisfies the following boundary condition:

$$\phi_i(x, r; \xi_i, \rho_i) \to 0 \qquad (x^2 + r^2 \to \infty) \tag{7}$$

To satisfy the boundary conditions in the far field, the solution $G(x, r)$ given by Lamb,[17] which describes the potential flow through an orifice in a rigid plate, is supplemented. The final expression of the velocity potential is as follows:

$$\phi(x, r) = \sum_{i=1}^{N} \phi_i(x, r; \xi_i, \rho_i) + C(t)G(x, r) \tag{8}$$

where

$$G(x, r) = \begin{cases} 1 - \dfrac{1}{\pi}\displaystyle\int_0^\infty k^{-1}\sin k\exp(kx)J_0(kr)\,\mathrm{d}k & (x < 0) \\ \dfrac{1}{\pi}\displaystyle\int_0^\infty k^{-1}\sin k\exp(-kx)J_0(kr)\,\mathrm{d}k & (x > 0) \end{cases}$$

and $C(t)$ is a time-dependent variable that will be determined in Sec. II.C. The axial and radial velocity are given by the derivatives of the velocity potential; that is,

$$u = \frac{\partial\phi}{\partial x}, \qquad v = \frac{\partial\phi}{\partial r} \tag{9}$$

Then

$$u(x, r) = \sum_{i=1}^{N} H(x\xi_i)U_i^V(x, r; \xi_i, \rho_i) + \sum_{i=1}^{N} H(x\xi_i)\hat{U}_i^V(x, r; \xi_i, \rho_i) + \sum_{i=1}^{N} U_i^A(x, r; \xi_i, \rho_i) + C(t)U^p(x, r) \tag{10}$$

$$v(x, r) = \sum_{i=1}^{N} H(x\xi_i)V_i^V(x, r; \xi_i, \rho_i) + \sum_{i=1}^{N} H(x\xi_i)\hat{V}_i^V(x, r; \xi_i, \rho_i) + \sum_{i=1}^{N} V_i^A(x, r; \xi_i, \rho_i) + C(t)V^p(x, r) \tag{11}$$

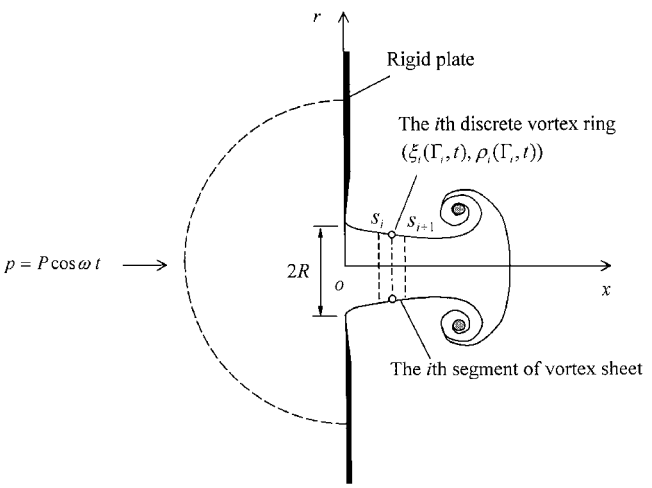

Fig. 1 Discretization of the shed vortex sheet at an orifice in a plate.

where

$$U_i^V(x, r; \xi_i, \rho_i) = -\frac{\Gamma_i}{2\pi r}\left\{\left(\frac{r-\rho_i}{R_1} + \frac{r+\rho_i}{R_2}\right)\times\left[K(\lambda) - \frac{1}{1-\lambda^2}E(\lambda)\right] - \left(\frac{\lambda}{1-\lambda^2}\right)\left(\frac{r-\rho_i}{R_1} - \frac{r+\rho_i}{R_2}\right)E(\lambda)\right\} \quad (12)$$

$$\hat{U}_i^V(x, r; \xi_i, \rho_i) = \frac{\Gamma_i}{2\pi r}\left\{\left(\frac{r-\rho_i}{\hat{R}_1} + \frac{r+\rho_i}{\hat{R}_2}\right)\times\left[K(\hat{\lambda}) - \frac{1}{1-\hat{\lambda}^2}E(\hat{\lambda})\right] - \left(\frac{\hat{\lambda}}{1-\hat{\lambda}^2}\right)\left(\frac{r-\rho_i}{\hat{R}_1} - \frac{r+\rho_i}{\hat{R}_2}\right)E(\hat{\lambda})\right\} \quad (13)$$

$$V_i^V(x, r; \xi_i, \rho_i) = -\frac{\Gamma_i}{2\pi}\frac{(x-\xi_i)}{r}\left(\frac{1}{R_1} + \frac{1}{R_2}\right)\times\left[K(\lambda) - \frac{1+\lambda^2}{1-\lambda^2}E(\lambda)\right] \quad (14)$$

$$\hat{V}_i^V(x, r; \xi_i, \rho_i) = \frac{\Gamma_i}{2\pi}\frac{(x-\xi_i)}{r}\left(\frac{1}{\hat{R}_1} + \frac{1}{\hat{R}_2}\right)\times\left[K(\hat{\lambda}) - \frac{1+\hat{\lambda}^2}{1-\hat{\lambda}^2}E(\hat{\lambda})\right] \quad (15)$$

$$U_i^A(x, r; \xi_i, \rho_i) = \frac{1}{\pi}\Gamma_i\rho_i\int_0^\infty\int_0^\infty\int_0^1 \exp(-k|x| - \lambda|\xi_i|)\times J_0(kr)J_1(\lambda\rho_i)k\cos ks\cos\lambda s\,\mathrm{d}s\,\mathrm{d}\lambda\,\mathrm{d}k \quad (16)$$

$$V_i^A(x, r; \xi_i, \rho_i) = \frac{1}{\pi}\,\mathrm{sgn}(x)\Gamma_i\rho_i\int_0^\infty\int_0^\infty\int_0^1 \exp(-k|x| - \lambda|\xi_i|)\times J_1(kr)J_1(\lambda\rho_i)k\cos ks\cos\lambda s\,\mathrm{d}s\,\mathrm{d}\lambda\,\mathrm{d}k \quad (17)$$

$$U^P(x, r) = -\frac{1}{\pi}\int_0^\infty \sin k\exp(-k|x|)J_0(kr)\,\mathrm{d}k \quad (18)$$

$$V^P(x, r) = -\mathrm{sgn}(x)\frac{1}{\pi}\int_0^\infty \sin k\exp(-k|x|)J_1(kr)\,\mathrm{d}k \quad (19)$$

In the preceding equations, $R_{1,2}^2 = (r-\rho_i)^2 + (x \mp \xi_i)^2$, $\hat{R}_{1,2}^2 = (r-\rho_i)^2 + (x \pm \xi_i)^2$, $\lambda = (R_2 - R_1)/(R_2 + R_1)$, and $\hat{\lambda} = (\hat{R}_2 - \hat{R}_1)/(\hat{R}^2 + \hat{R}_1)$ and $K(y)$ and $E(y)$ are, respectively, the complete elliptic integrals of the first and second kind. The evaluations of the integrals in Eqs. (16) and (17) are presented in Appendix A. Equations (18) and (19) can be analytically integrated according to Watson.[18]

Noted that, when Eqs. (10) and (11) are used to calculate the convection velocity of the jth discrete vortex ring, the induced velocity due to itself is not considered; that is,

$$u(x_j, r_j) = \sum_{\substack{i=1\\ i\neq j}}^{N} H(x_j\xi_i)U_i^V(x_j, r_j; \xi_i, \rho_i) + \sum_{i=1}^{N} H(x_j\xi_i)\hat{U}_i^V(x_j, r_j; \xi_i, \rho_i) + \sum_{i=1}^{N} U_i^A(x_j, r_j; \xi_i, \rho_i) + C(t)U^p(x_j, r_j) \quad (20)$$

$$v(x_j, r_j) = \sum_{\substack{i=1\\ i\neq j}}^{N} H(x_j\xi_i)V_i^V(x_j, r_j; \xi_i, \rho_i) + \sum_{i=1}^{N} H(x_j\xi_i)\hat{V}_i^V(x_j, r_j; \xi_i, \rho_i) + \sum_{i=1}^{N} V_i^A(x_j, r_j; \xi_i, \rho_i) + C(t)V^p(x_j, r_j) \quad (21)$$

In fact, the jth discrete vortex ring represents a small segment of the axisymmetric vortex sheet, and it has an axial self-induced velocity u_I. Therefore, this self-induced velocity must be included in the convection velocity. The self-induced velocity of the jth discrete vortex ring is calculated according to Sugiaka and Widnall.[19]

$$u_I(\xi_j, \rho_j) = (\Gamma_j/4\pi\rho_j)\left[\ln(8\rho_j/\sigma_j) - \tfrac{1}{4}\right] \quad (22)$$

where σ_j is the core radius of the jth discrete vortex ring, which is calculated from the following relation given in Ref. 19:

$$\sigma_j \approx 0.25\Delta_j \quad (23)$$

where Δ_j is the length of the jth vortex sheet segment that will be determined in Sec. II.B. Note that the core radius σ_j results from the discretization of the continuous vortex sheet, and so it is not a physical one.

B. Kutta Condition

As shown in Fig. 2, the nascent vortex ring represents a small segment of vortex sheet EP that starts from the sharp edge E. In the present model, the starting vortex sheet is chosen from a small segment of the steady jet. To obtain smooth flow near the sharp edge, the starting vortex sheet is subdivided into N_1 subpanels of equal length. Each subpanel is represented by a subvortex ring (ξ_{1j}, ρ_{1j}) with circulation Γ_1/N_1. The circulation of the nascent vortex ring is determined by the Kutta condition, which requires

$$u(0, 1^-) = 0 \quad (24)$$

To satisfy this condition, Γ_1 is given by the following relation:

$$\frac{\Gamma_1}{N_1} = \left[C(t) - \sum_{i=2}^{N}\Gamma_i K_i(\xi_i, \rho_i)\right] \Bigg/ \sum_{j=1}^{N_1} K_j(\xi_{1j}, \rho_{1j}) \quad (25)$$

where

$$K_i(\xi_i, \rho_i) = \rho_i\int_0^\infty \exp(-k|\xi_i|)J_1(k\rho_i)\cos k\,\mathrm{d}k$$

and it can be analytically integrated according to Ref. 18. The derivation of Eq. (25) is presented in Appendix B. The circulation shedding rate at the orifice edge is

$$\frac{\mathrm{d}\Gamma}{\mathrm{d}t} = \frac{1}{2}\left(v_-^2 - v_+^2\right) \quad (26)$$

where v_- and v_+ are slip velocities at the two sides of the orifice edge. To calculate v_- and v_+, the contribution of the first discrete

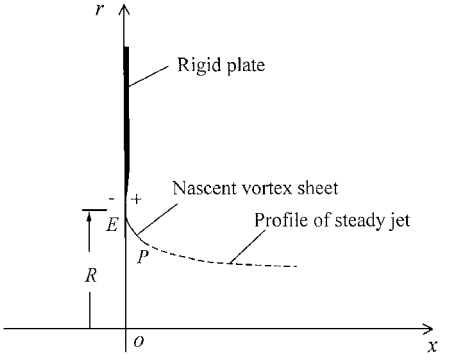

Fig. 2 Geometry of the starting vortex sheet *EP*.

vortex ring Γ_1 will be substituted by that of the N_1 subdiscrete vortex rings with circulation Γ_1/N_1. Then, Eq. (11) is rewritten as

$$v(x,r) = \sum_{j=1}^{N_1} H(x\xi_{1j})\left[V_{1j}^V(x,r;\xi_{1j},\rho_{1j}) + \hat{V}_{1j}^V(x,r;\xi_{1j},\rho_{1j})\right] + \sum_{j=1}^{N_1} V_{1j}^A(x,r;\xi_{1j},\rho_{1j}) + \sum_{i=2}^{N} H(x\xi_i)\left[V_i^V(x,r;\xi_i,\rho_i) + \hat{V}_i^V(x,r;\xi_i,\rho_i)\right] + \sum_{i=2}^{N} V_i^A(x,r;\xi_i,\rho_i) + C(t)V^p(x,r) \tag{27}$$

The slip velocities v_- and v_+ are calculated from Eq. (27):

$$v_- = v(-\varepsilon_x, 1+\varepsilon_r), \qquad v_+ = v(\varepsilon_x, 1+\varepsilon_r) \tag{28}$$

where $\varepsilon_x \sim \mathcal{O}(10^{-2})$ and $\varepsilon_r \sim \mathcal{O}(10^{-2})$. The procedure to calculate the circulation of the nascent vortex and the length of the starting vortex sheet is similar to that of Ref. 13.

1) A value of Δ_1 is chosen, which is the length of the starting vortex sheet. The coordinates of the subvortex rings (ξ_{1j}, ρ_{1j}) are calculated.

2) The circulation of the nascent vortex Γ_1^K is calculated from Eq. (25).

3) The slip velocities are calculated from Eq. (28), and the circulation of the nascent vortex Γ_1^V is calculated according to Eq. (26):

$$\Gamma_1^V = \tfrac{1}{2}\left(v_-^2 - v_+^2\right)\Delta t \tag{29}$$

4) Repeat the calculations in steps 1–3 until the following condition is fulfilled:

$$\left|\Gamma_1^K - \Gamma_1^V\right| \Big/ \left|\Gamma_1^V\right| < \varepsilon \tag{30}$$

where ε is a control error. Then, Γ_1^V and Δ_1 are employed as the required value. If the calculation does not converge after 20 iterations, the values of Γ_1^V and Δ_1 in the last iteration are employed.

C. Determination of $C(t)$

As shown in Fig. 3, the pressure difference between the two sides of the plate can be calculated using Bernoulli equation along the path A–E–B, where A and B are two points in the far field at the two sides of the plate, and $E(0, 1^-)$ is the edge point:

$$p_A - p_B = \frac{1}{2}\left(v_-^2 - v_+^2\right) + \frac{\partial}{\partial t}\int_A^B \boldsymbol{w}\cdot \mathrm{d}\boldsymbol{s} \tag{31}$$

where $\boldsymbol{w} = (u, v)$, $\mathrm{d}\boldsymbol{s} = (\mathrm{d}x, \mathrm{d}r)$. The following conditions are employed to derive Eq. (31):

$$|\boldsymbol{w}_A| = 0, \qquad |\boldsymbol{w}_B| = 0, \qquad \left(\sqrt{x^2+r^2} \to \infty\right)$$
$$p(0^+, 1^-) = p(0^-, 1^-) \tag{32}$$

which mean the velocity is zero in the far field and the pressure is continuous across the vortex sheet at the edge. By the use of the relation

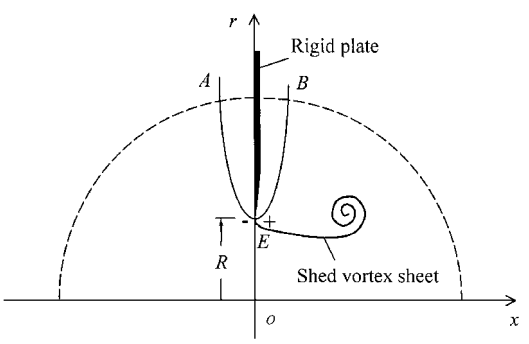

Fig. 3 Path A–E–B along which the Bernoulli equation is applied.

$$C(t) = -\int_A^B \boldsymbol{w}\cdot \mathrm{d}\boldsymbol{s} \tag{33}$$

and of Eq. (26), Eq. (31) can be rewritten as

$$P\cos t = \frac{\mathrm{d}\Gamma}{\mathrm{d}t} - \frac{\mathrm{d}}{\mathrm{d}t}C(t) \tag{34}$$

By use of the initial condition $\Gamma(0) = 0$, the integration of Eq. (34) with respect to time t gives

$$C(t) = -P\sin t + \Gamma(t) \tag{35}$$

where $\Gamma(t)$ is the total amount of circulation that has shed into the flowfield from the orifice edge at time t.

D. Convection of the Vortex Sheet

Equation (2), which governs the motion of the discrete vortex rings, is solved by the second-order Runge–Kutta scheme:

$$K_1 = \frac{\mathrm{d}Z}{\mathrm{d}t}(Z_t, t)\Delta t, \qquad K_2 = \frac{\mathrm{d}Z}{\mathrm{d}t}(Z_t + K_1, t+\Delta t)\Delta t$$
$$Z_{t+\Delta t} = Z_t + \frac{1}{2}(K_1 + K_2) \tag{36}$$

where $Z = (\xi_i, \rho_i)^T$, $1 \le i \le N$. The mth time step is described as follows.

1) Evaluate $C(t_{m-1})$ from Eq. (35). The total amount of circulation of the shed vortex sheet is approximately given by

$$\Gamma(t_{m-1}) = \sum_{i=0}^{m-2} \Gamma_1(t_i) \tag{37}$$

where $m-1$ is the number of the completed time steps and

$$t_i = t_0 + i\Delta t \tag{38}$$

where t_0 is an initial time of a small value, which is selected at the beginning of all of the time steps. The initial condition is approximately given by $\Gamma(t_0) = 0$.

2) Calculate the circulation, position, and core radius of the nascent vortex ring.

3) Calculate the new positions of the discrete vortex rings according to Eq. (36).

4) The time t_{m-1} is incremented by Δt, where $t_m = t_{m-1} + \Delta t$. Prepare for the next time step by changing the indices of the discrete vortex rings as follows:

$$\Gamma_{i+1} = \Gamma_i, \qquad \xi_{i+1} = \xi_i, \qquad \rho_{i+1} = \rho_i, \qquad \sigma_{i+1,} = \sigma_i \tag{39}$$

To limit the computation time as the calculation proceeds, an amalgamation process is introduced. When the number of the discrete vortex rings exceeds M, the amalgamation process begins. The earliest shed vortex ring is chosen to be the amalgamation center, and the vortex rings shed later are amalgamated with it in such a way that one is absorbed after each time step. Usually the amalgamation happens somewhere far away from the orifice. Ignoring the influence of the rigid plate, the circulation and the position of the new vortex ring after amalgamation is calculated from the following relation, given in Ref. 17:

$$\Gamma_{M,\mathrm{new}} = \Gamma_M + \Gamma_{M-1}$$
$$\xi_{M,\mathrm{new}} = \frac{\Gamma_M\rho_M^2\xi_M + \Gamma_{M-1}\rho_{M-1}^2\xi_{M-1}}{\Gamma_M\rho_M^2 + \Gamma_{M-1}\rho_{M-1}^2}$$
$$\rho_{M,\mathrm{new}} = \frac{\Gamma_M\rho_M + \Gamma_{M-1}\rho_{M-1}}{\Gamma_M + \Gamma_{M-1}} \tag{40}$$

The amalgamation proceeds until Γ_{M-1} changes sign. The amalgamation center represents a physical vortex ring that is formed by the rolling up of the vortex sheet. Thus, one physical vortex ring is

formed after each half-cycle. A physical vortex ring has a finite core radius that is given by the following relation, according to Sallet and Widmayer.[20]

$$\sigma_c = 2\sqrt{\nu t_c} \tag{41}$$

where $t_c = T/2$. The self-induced velocity of a physical vortex ring is calculated from Eq. (22), according to Ref. 17. The numerical tests show that the variations of the core radius σ_c have little influence on the final numerical results. Therefore, the results of the present model are basically independent of viscosity.

E. Volume Flux

The volume flux through the orifice is given by

$$Q(t) = 2\pi \int_0^1 \frac{\partial \phi}{\partial x}(0^+, r) r \, dr \tag{42}$$

Equation (42) can be analytically integrated according to Ref. 16, then

$$Q(t) = \sum_{i=1}^{N} Q_i(\xi_i, \rho_i) - 2C(t) \tag{43}$$

where

$$Q_i(\xi_i, \rho_i) = 2\Gamma_i \left\{1 + \left[\left(\xi_i^2 + \rho_i^2 - 1\right)^2 + 4\xi_i^2\right]^{\frac{1}{4}} \sin(\alpha/2)\right\}$$

and

$$\alpha = \begin{cases} \arctan\left[-2|\xi_i| \Big/ \left(\rho_i^2 + \xi_i^2 - 1\right)\right] & \left(\rho_i^2 + \xi_i^2 > 1\right) \\ -\pi/2 & \left(\rho_i^2 + \xi_i^2 = 1\right) \\ -\pi + \arctan\left[-2|\xi_i| \Big/ \left(\rho_i^2 + \xi_i^2 - 1\right)\right] & \left(\rho_i^2 + \xi_i^2 < 1\right) \end{cases}$$

III. Results and Discussion

From the preceding analysis, we know that the theoretical results depend only on the non-dimensional amplitude of the applied sound pressure. The vortex shedding process for $\bar{P} = 5.0$, $\Delta\bar{t} = 0.0261$, and $M = 50$ is shown in Fig. 4. The evolution of the shed vortex sheet is calculated qualitatively, and the rolling up nature of the shed vortex sheet is clearly demonstrated by the numerical simulation. The forming process of the vena contracta is also shown in Fig. 4, and the results in Figs. 4a–4h indicate that both the position and the contraction value of the vena contracta are time dependent. The filled and open circles indicate the vortex strength is positive and negative, respectively. In Figs. 4d and 4g, the amalgamation centers are marked by open squares. In Figs. 4e and 4h the amalgamation process has been completed, but the formed physical vortex rings do not appear because they are out of the maximum range of the figures. It is shown that a smoothing rolling up is always obtained in the vicinity of the orifice. However, the motion of the discrete vortex rings tends to be irregular in the flowfield two or three radius away from the orifice. At such a distance, the vortex sheet has been considerably stretched, and a limited number of discrete vortex rings (for example, $M = 50$) is not enough to represent it. To obtain a smoothing vortex sheet far from the orifice, a procedure is needed to redistribute the vortex strength. Such a procedure is not incorporated in the present method because we assume that the acoustic nonlinearity of an orifice mainly depends on the motion of the vortex sheet near to the orifice.

Figures 5a and 6a show, respectively, the calculated time history of the average velocity through the orifice for $\bar{P} = 5.0$ and 50.0. It is shown that $\bar{u}_{\text{av}}$ is almost convergent after one cycle. In Figs. 5a and 6a the nonlinear distortion of the velocity has appeared because the velocity curves are periodic but nonsinusoidal when it is convergent. The Fourier decomposition of $\bar{u}_{\text{av}}$ can be expressed as follows:

$$\bar{u}_{\text{av}}(\bar{t}) = \sum_{n=1}^{\infty} \bar{U}(n) \cos[n\bar{t} + \phi(n)] \tag{44}$$

The first six harmonics of $\bar{u}_{\text{av}}$ for $\bar{P} = 5.0$ and 50.0 are shown in Figs. 5b and 6b, respectively. We can see that the first, third, and fifth harmonics play a dominant role in both Figs. 5b and 6b. The distortion of the average velocity can be analyzed from its spectrum. In Fig. 5b, $U(1)$ is 12.8 times as large as $U(3)$, and it is 137.3 times as large as $U(5)$. In Fig. 6b, $U(1)$ is 7.56 times as large as $U(3)$, and it is 20.2 times as large as $U(5)$. It seems to show that the amplitudes of the higher harmonics increase with the increasing amplitude

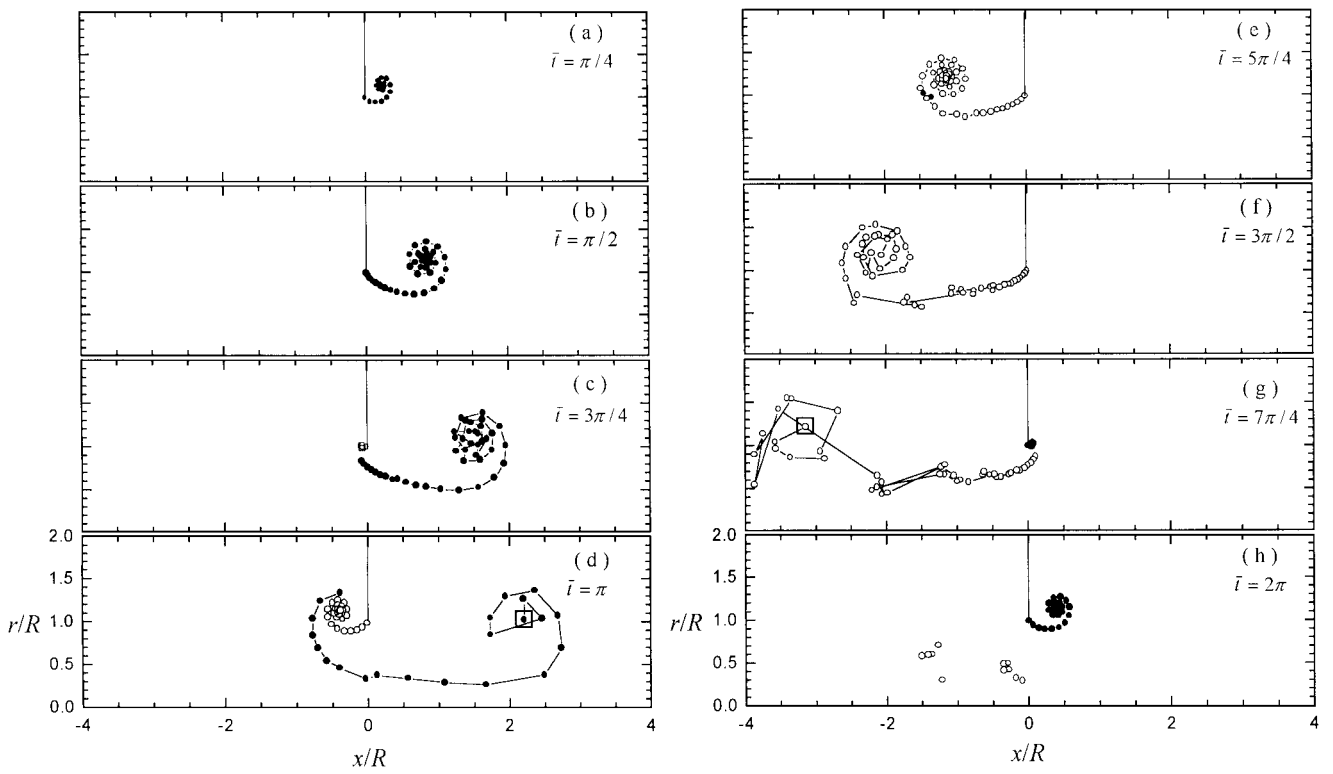

Fig. 4 Computed vortex shedding process at the edge of an orifice, where the coordinate of the orifice edge is (0, 1); first period is shown at every one-eighth cycle.

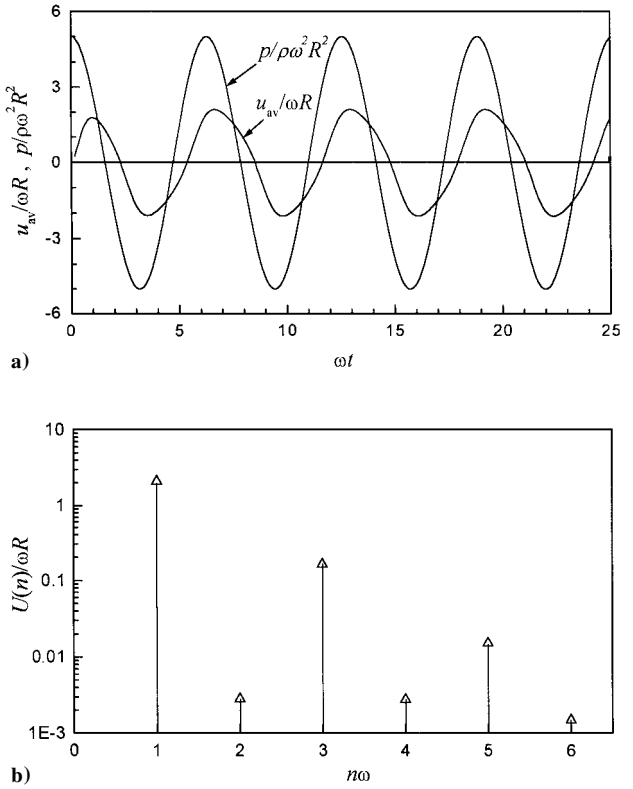

Fig. 5 Average velocity through the orifice for $\bar{P} = 50.0$: a) time history, $\bar{p} = \bar{P}\cos\omega t$; and b) spectrum, where $U(n)$ is the amplitude of nth harmonic of the average velocity.

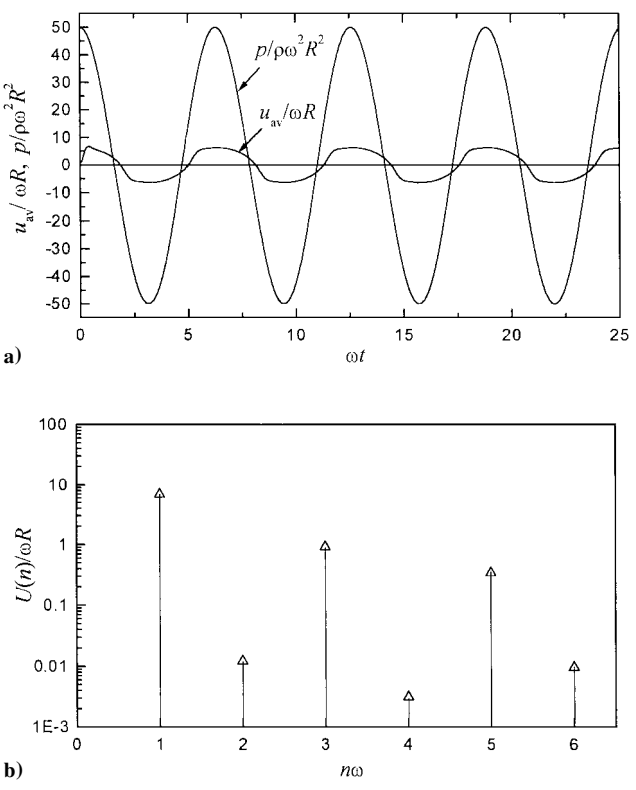

Fig. 6 Average velocity through the orifice for $\bar{P} = 50.0$: a) time history, $\bar{p} = \bar{P}\cos\omega t$; and b) spectrum, where $U(n)$ is the amplitude of nth harmonic of the average velocity.

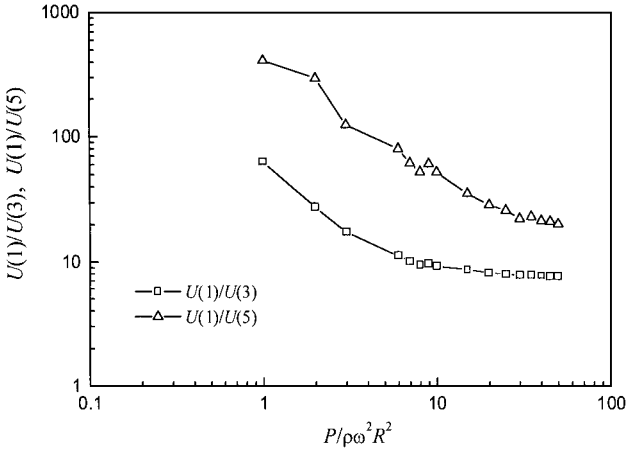

Fig. 7 Ratio between the amplitude of the fundamental harmonic and that of the third harmonic or fifth harmonic as a function of the amplitude of the applied sound pressure.

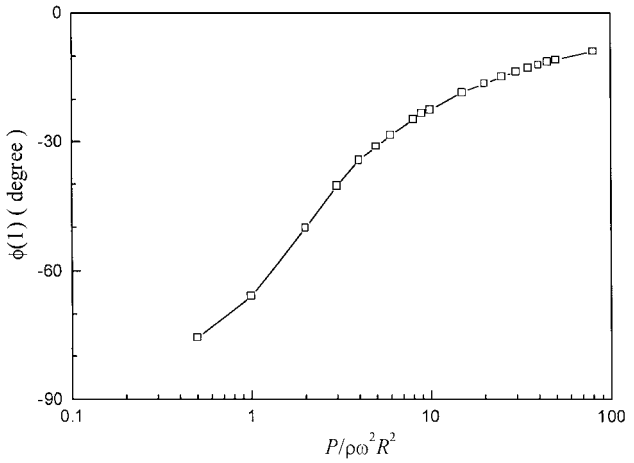

Fig. 8 Phase angle of the first harmonic of the average velocity through the orifice as a function of the amplitude of the applied sound pressure.

of the applied pressure. However, further investigations show that the ratios between the amplitude of the fundamental harmonic and that of higher-order harmonics gradually tend to certain limits when $\bar{P} > 30.0$, as shown in Fig. 7. Therefore, it can be deduced that the distortion of the average velocity nearly remains unchanged on such a condition. When $\bar{P} = 50.0$, $U(1)/U(3)$ and $U(1)/U(5)$ are equal to 7.56 and 20.2, respectively. These values are near to $U(1)/U(3) = 7$ and $U(1)/U(5) = 15.4$, which were obtained by Ingard[3] on the quasi-steady assumption. In the present paper, the specific acoustic impedance is normalized by $\rho\omega R$. The nonlinear acoustic impedance of an orifice is defined in terms of the fundamental harmonic of u_{av} according to Ref. 1. The normalized specific acoustic impedance of an orifice is given by the following relation:

$$z_r = \bar{P}\cos[\phi(1)]/\bar{U}(1), \qquad z_x = \bar{P}\sin[\phi(1)]/\bar{U}(1) \quad (45)$$

In Fig. 8, $\phi(1)$ is plotted as a function of the amplitude of the applied sound pressure (the phase of the applied sound pressure has been selected to be zero). Figure 8 shows that the phase of the fundamental harmonic of the average velocity decreases as the sound pressure amplitude increases. This result is consistent with the experimental data presented in Ref. 1. In Fig. 9, the normalized specific acoustic impedance is calculated as a function of the amplitude of the applied sound pressure. It is shown that the normalized specific acoustic resistance increases markedly while the normalized specific acoustic reactance decreases with the increase of the nondimensional amplitude of the applied sound pressure. As we know, the linear value of the normalized specific acoustic reactance is 1.7. The results of Fig. 9 show that the normalized specific acoustic reactance is

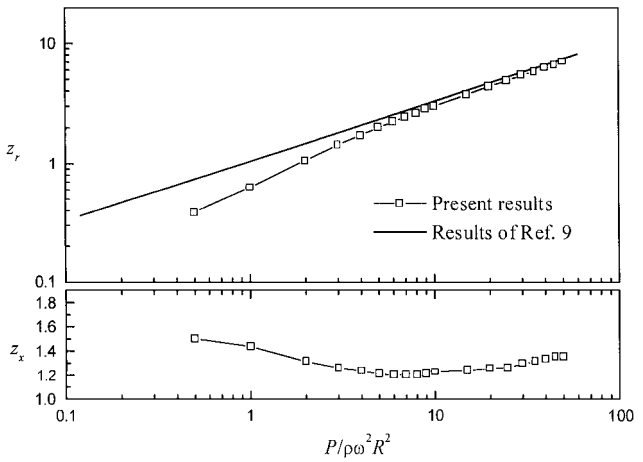

Fig. 9 Normalized specific acoustic impedance as a function of the amplitude of the applied sound pressure: a) normalized specific acoustic resistance, results of Ref. 9 calculated for $C_c = 0.61$; and b) normalized specific acoustic reactance.

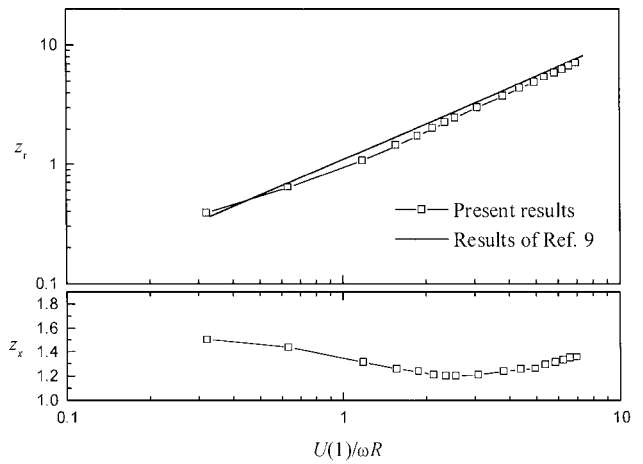

Fig. 10 Normalized specific acoustic impedance as a function of the amplitude of the first harmonic of the average velocity through the orifice: a) normalized specific acoustic resistance, results of Ref. 9 calculated for $C_c = 0.61$; and b) normalized specific acoustic reactance.

approaching this value when the nondimensional amplitude of the sound pressure is very low. As $\bar{P}$ increases, the normalized specific acoustic reactance decreases to 0.71 of its linear value at its lowest point. This result is in excellent agreement with the ratio 0.7 obtained by Thurston et al.[4] However, it is much higher than the ratio 0.5 proposed by Ingard and Ising.[1]

In Fig. 10, the normalized specific acoustic impedance is plotted as a function of $\bar{U}(1)$, which is the nondimensional amplitude of the fundamental harmonic of the average velocity. The results of Fig. 10 show that the normalized specific acoustic resistance is proportional to $\bar{U}(1)$, as revealed by the previous experiment.[1] In Figs. 9a and 10a, a comparison is made between the present numerical results and the quasi-steady results of Ref. 9. The results of Ref. 9 are obtained for vena contracta coefficient $C_c = 0.61$. No empirical parameter such as the vena contracta coefficient is introduced in the present model. However, the present numerical results of the normalized specific acoustic resistance are in good agreement with the quasi-steady results of Ref. 9, as shown in Figs. 9a and 10a.

Conclusion

The nonlinear acoustic properties of an orifice have long received attention. This paper presents an axisymmetric potential model in an attempt to explain certain phenomena observed in the previous experiments. As revealed by the previous investigations, the nonlinear acoustic properties of an orifice are closely related to the vortex shedding process occurring at the edge of the orifice. However, at present, there is little effort to study theoretically the vortex motion in detail aiming at giving more insight into the acoustic nonlinearity of an orifice. In the present paper, a discrete vortex method is employed to describe the vortex motion around an orifice. Some characteristic phenomena, such as the rolling up of the shed vortex sheet and the forming of the vena contracta, are simulated. At high sound pressure level, the distortion of the velocity in an orifice is also one of the nonlinear characteristics of great concern. When the applied sound pressure is harmonic, both the time history and spectrum of the average velocity through the orifice are obtained numerically. Also, the distortion of the velocity is investigated by analyzing the distribution of the harmonics in the computed spectrum. Because of its importance in the design of Helmholtz resonators, the calculation of the nonlinear acoustic impedance becomes an object of most concern when studying the nonlinear acoustic phenomena occurring at an orifice. We adopt a numerical approach to calculate the nonlinear acoustic impedance. It is found that the computed nonlinear acoustic resistance is in good agreement with the previous models based on the quasi-steady assumption.[9] Compared with the acoustic resistance, it proves more difficult to calculate the nonlinear acoustic reactance that is associated with the attached mass. To the authors' knowledge, this problem has not been well solved so far. As one of the major purposes of the present paper, a numerical procedure is used to compute the nonlinear acoustic reactance over a wide range of sound pressure amplitude. The numerical results show that the nonlinear acoustic reactance decreases with the increasing amplitude of the applied sound pressure, which is consistent with the previous experiments.[1,2,4] The acoustic reactance decreases to 0.71 of its linear value at its lowest point. This result is also in good agreement with the previous experimental data 0.7 (Ref. 4). Because the viscosity is of little importance in the present model, the numerical results reconfirm the conclusion that the absorption mechanism is the conversion of acoustic energy into vortical energy.[9]

Appendix A: Evaluations of the Multiple Integrals in Eqs. (16) and (17)

The integration of Eqs. (16) and (17) over k and λ results in the following expressions:

$$U_i^A = \frac{1}{\pi}\Gamma_i \int_0^1 \left\{(|x| - is)[(|x| - is)^2 + r^2]^{-\frac{3}{2}}\right\} \times \left\{1 - (|\xi_i| - is)\left[(|\xi_i| - is)^2 + \rho_i^2\right]^{-\frac{1}{2}}\right\} \mathrm{d}s \tag{A1}$$

$$V_i^A = \frac{1}{\pi}\mathrm{sgn}(x)\rho_i\Gamma_i \int_0^1 \left\{[(|x| - is)^2 + r^2]^{-\frac{3}{2}}\right\} \times \left\{1 - (|\xi_i| - is)\left[(|\xi_i| - is)^2 + \rho_i^2\right]^{-\frac{1}{2}}\right\} \mathrm{d}s \tag{A2}$$

Note that only the real parts in the parentheses are considered in these equations. The integration of Eq. (A1) or Eq. (A2) over s is carried out by means of a numerical method. On the condition that $|x|$ or $|\xi_i|$ has a small value, the integrated functions in Eqs. (A1) and (A2) have high peaks, and so an adaptive integration program is employed to accelerate the convergence.

Appendix B: Derivation of Eq. (25)

A method similar to that of Dowling[21] is employed to derive Eq. (25). Considering the arrangement shown in Fig. 1, the presence of the orifice can be represented by a distribution of sources lying on the disk $x = 0^+$ and $r < 1$ according to Ref. 16. If it is assumed that $F_i(x, r)$ is the potential function generated by the distributed sources, the following expression can be obtained:

$$F_i(0^+, r) = \frac{1}{2}C(t) - \frac{1}{2}\Gamma_i\rho_i \int_0^\infty \exp(-k|\xi_i|)J_0(kr)J_1(k\rho)\,\mathrm{d}k \tag{B1}$$

The strength of the sources is equal to the normal velocity in the orifice, and so the results of Copson (see Ref. 22) can be used to give the normal velocity; that is,

$$u_i(0^+, r) = \frac{C(t)}{2\pi\sqrt{1-r^2}} - \frac{1}{2}\Gamma_i\rho_i \int_0^\infty \exp(-k|\xi_i|) J_1(k\rho_i) \times \left[\frac{1}{2}kJ_0(kr) + \frac{1}{\pi}\int_1^\infty \frac{t\cos kt}{\sqrt[3]{t^2-r^2}}\,\mathrm{d}t\right]\mathrm{d}k \tag{B2}$$

Integrating the t integral by parts leads to

$$u_i(0^+, r) = \frac{1}{2\pi\sqrt{1-r^2}}\left[C(t) - \Gamma_i\rho_i \times \int_0^\infty \exp(-k|\xi_i|) J_1(k\rho_i)\cos k\,\mathrm{d}k\right] - \frac{1}{4}\Gamma_i\rho_i \int_0^\infty k\exp(-k|\xi_i|) J_1(k\rho_i) \times \left[J_0(kr) - \int_1^\infty \frac{\sin kt}{\sqrt{t^2-r^2}}\,\mathrm{d}t\right]k\,\mathrm{d}k \tag{B3}$$

Note that the first term of Eq. (B3) has a square-root singularity. To remove the singularity, the following condition must be satisfied:

$$C(t) - \Gamma_i\rho_i \int_0^\infty \exp(-k|\xi_i|) J_1(k\rho_i)\cos k\,\mathrm{d}k = 0 \tag{B4}$$

On the condition of Eq. (B4), it is easy to prove that

$$u_i(0^+, 1^-) = 0 \tag{B5}$$

Based on these results, the derivation of Eq. (25) is straightforward.

Acknowledgment

The financial support of National Natural Science Foundation of China (No. 599-5616) is gratefully acknowledged.

References

[1]Ingard, U., and Ising, H., "Acoustic Nonlinearity of an Orifice," *Journal of the Acoustical Society of America*, Vol. 42, No. 1, 1967, pp. 6–17.

[2]Ingard, U., and Labate, S., "Acoustic Circulation Effects and the Nonlinear Impedance of Orifices," *Journal of the Acoustical Society of America*, Vol. 22, No. 2, 1950, pp. 211–218.

[3]Ingard, U., "Nonlinear Distortion of Sound Transmitted through an Orifice," *Journal of the Acoustical Society of America*, Vol. 48, No. 1, 1970, pp. 32, 33.

[4]Thurston, G. B., Hargrove, L. E., Jr., and Cook, B. D., "Nonlinear Properties of Circular Orifices," *Journal of the Acoustical Society of America*, Vol. 29, No. 9, 1957, pp. 992–1001.

[5]Salikuddin, M., and Ahuja, K. K., "Acoustic Power Dissipation on Radiation Through Duct Terminations: Experiments," *Journal of Sound and Vibration*, Vol. 91, No. 4, 1983, pp. 479–502.

[6]Howe, M. S., "On the Theory of Unsteady High Reynolds Number Flow Through a Circular Aperture," *Proceedings of the Royal Society of London, Series A: Mathematical and Physical Sciences*, Vol. 366, No. 1724, 1979, pp. 205–233.

[7]Howe, M. S., "The Dissipation of Sound at an Edge," *Journal of Sound and Vibration*, Vol. 70, No. 3, 1980, pp. 407–411.

[8]Bechert, D. W., "Sound Absorption Caused by Vorticity Shedding, Demonstrated with a Jet Flow," *Journal of Sound and Vibration*, Vol. 70, No. 3, pp. 389–405.

[9]Cummings, A., and Eversman, W., "High Amplitude Acoustic Transmission Through Duct Terminations: Theory," *Journal of Sound and Vibration*, Vol. 91, No. 4, 1983, pp. 503–518.

[10]Hersh, A. S., and Rogers, T., "Fluid Mechanical Model of the Acoustic Impedance of Small Orifices," AIAA Paper 75-495, March 1975.

[11]Melling, T. H., "The Acoustic Impedance of Perforates at Medium and High Sound Pressure Levels," *Journal of Sound and Vibration*, Vol. 29, No. 1, 1973, pp. 1–63.

[12]Evans, R. A., and Bloor, M. I. G., "The Starting Mechanism of Wave-Induced Flow Through a Sharp-Edged Orifice," *Journal of Fluid Mechanics*, Vol. 82, 1977, pp. 115–128.

[13]Kiya, M., Sasaki, K., and Arie, M., "Discrete Vortex Simulation of a Turbulent Separation Bubble," *Journal of Fluid Mechanics*, Vol. 120, 1982, pp. 219–244.

[14]Peters, M. C. A. M., and Hirschberg, A., "Acoustically Induced Periodic Vortex Shedding at Sharp Edged Open Channel Ends: Simple Vortex Models," *Journal of Sound and Vibration*, Vol. 161, No. 2, pp. 281–299.

[15]Disselhorst, J. H. M., and Van Wijingaarden, L., "Flow in the Exit of Open Pipes During Acoustic Resonance," *Journal of Fluid Mechanics*, Vol. 99, 1980, pp. 293–319.

[16]Miloh, T., and Shlien, D. J., "Passage of a Vortex Ring Through a Circular Aperture in an Infinite Plane," *Physics of Fluids*, Vol. 20, No. 8, 1977, pp. 1219–1227.

[17]Lamb, H., *Hydrodynamics*, Cambridge Univ. Press, Cambridge, England, U.K., 1975, pp. 137–139, 239.

[18]Watson, G. N., *A Treatise on the Theory of Bessel Functions*, Cambridge Univ. Press, Cambridge, England, U.K., 1944.

[19]Sugiaka, I., and Widnall, S. E., "A Panel Method Study of Vortex Sheets with Special Emphasis on Sheets of Axisymmetric Geometry," NASA CR-177365, 1985.

[20]Sallet, D. W., and Widmayer, R. S., "An Experimental Investigation of Laminar and Turbulent Vortex Rings in Air," *Zeitschrift für Flugwissenschaften*, Vol. 22, No. 6, 1974, pp. 207–215.

[21]Dowling, A. P., "Vortex Sound Interaction," *2nd International Congress on Recent Developments in Air- and Structure-Borne Sound and Vibration*, Auburn Univ., Auburn, AL, Vol. 1, 1992, pp. 37–50.

[22]Sneddon, I. N., *Mixed Boundary Value Problems in Potential Theory*, North-Holland, Amsterdam, 1966, pp. 69–74.

P. J. Morris
Associate Editor